Probing the band structure of a two-dimensional hole gas using a one-dimensional superlattice

B. Brosh, M. Y. Simmons, S. N. Holmes,*A. R. Hamilton, D. A. Ritchie, and M. Pepper
Cavendish Laboratory, Madingley Road, Cambridge CB3 OHE, United Kingdom
(Received 12 June 1996)

Using a one-dimensional superlattice we have mapped out the Fermi surface of a two-dimensional (2D) hole gas in a GaAs/Al_xGa_{1-x}As heterojunction grown on the (311)*A* surface of GaAs. This follows our observation of commensurability magnetoresistance oscillations from a weakly one-dimensionally modulated (311)*A* 2D hole gas that is confined to square and triangular quantum wells. The dependence of the oscillations on the modulation direction in the (311)*A* plane reflects its known *k*-space anisotropy. This method is a minimally invasive probe of the Fermi surface of high-mobility 2D systems. [S0163-1829(96)50644-2]

In the presence of a weak one-dimensional (1D) lateral superlattice potential and perpendicular magnetic (B) fields, the resistivity ρ_{xx} of a two-dimensional electron gas (2DEG) along the modulation direction (x) displays oscillations periodic in B^{-1}.[1] Extrema in ρ_{xx} occur at fields satisfying the following commensuration condition between the electron classical cyclotron diameter $2R_C$ and the grating potential period a:

$$2R_C = 2\hbar k_F/eB = a(i+\phi), \quad i = 1,2, \ldots, \tag{1}$$

where k_F is the Fermi wave vector and ϕ is the deviation of these $2R_C$ values from integer multiples of the potential period. Those commensurability oscillations (CO's) were shown[2] to be due to a resonance between the electron orbital motion and the oscillating drift of the orbit center, occurring when Eq. (1) is satisfied. This model finds that the expression

$$\frac{\rho_{xx}(B)}{\rho_0(0)} = 1 + 2\left(\frac{eV_0}{E_F}\right)^2\left(\frac{l^2}{aR_C}\right)\cos^2\left(2\pi\frac{R_C}{a} - \frac{\pi}{4}\right) \tag{2}$$

reproduced the positions of electron CO extrema, when $2\pi R_C/a \ll 1$. Here, ρ_0 is the unmodulated 2D gas resistivity, V_0 is the modulation amplitude, l is the electron mean free path (MFP), and E_F is the Fermi energy. This predicts $\phi = \pm 0.25$ for maxima and minima in ρ_{xx}. In order to observe CO, the MFP of the carriers has to be sufficiently large, as shown by Eq. (2). Therefore, to date, CO have only been observed from 2DEG's [in (100)-oriented GaAs/Al_xGa_{1-x}As heterojunctions] due to the relatively high mobility of electrons compared to hole gases. Recently, however, high enough hole mobilities have been achieved using the (311)*A* surface of GaAs with Si as a *p*-type dopant. The (311)*A* plane mobilities, however, were found to be substantially anisotropic; higher mobilities were found along the $[\bar{2}33]$ directions than along $[0\bar{1}1]$.[3]

We report an observation of CO in the magnetoresistance (MR) of a weakly 1D modulated (311)*A* 2D hole gas. We further demonstrate a technique utilizing 1D superlattices which could, in principle, be used to determine the band structure of non-(100) indexed high-mobility 2D gases.

Two modulation-doped GaAs/Al_xGa_{1-x}As hole gas heterostructures, grown on the (311)*A* surface of GaAs, were used in this study. The first, *T*212, has a 277-nm deep (from the surface) heterojunction with a square quantum well (QW) and a 2D hole mobility (μ) of 75 $m^2V^{-1}s^{-1}$ at a hole density (p) of 1.8×10^{15} m^{-2}. The second, *T*97, has a 100-nm deep triangular shaped QW with $\mu = 50$ $m^2V^{-1}s^{-1}$ at $p = 2.1\times10^{15}$ m^{-2}. The mobility values were obtained from measuring the ungated Hall bars along the $[\bar{2}33]$ direction in the dark at 300 mK. Samples were prepared using conventional lithographic techniques to etch 20-μm-wide Hall-bar mesa with distances of 30 μm between longitudinal voltage probes. 50 nm of NiCr/Au was evaporated onto the surface of the mesa into patterns, each consisting of a 400-nm period grating and a perpendicularly crossing line (from outside the mesa), defined by standard electron-beam techniques. A subsequent lift-off process revealed a comb-shaped Schottky gate which fills the whole area between the probes with metal strips. In each device the long axis of the Hall bar was laid along a different crystallographic direction. Six directions between $[\bar{2}33]$ and $[0\bar{1}1]$ were used.

The larger effective mass $m^*(0.35m_e)$ of 2D hole gases (2DHG),[4] compared to electrons, increases the system's density of states such that the condition[5] $k_BT \leq \hbar\omega_c k_F a/2$, where $\omega_c = (eB/m^*)$, for CO oscillations to be observed, is made more severe. An excitation current of 10 nA was used, parallel to the potential modulation and the samples were cooled to ≤ 4.2 K before measuring the longitudinal and transverse MR beneath the gate area (using standard four-terminal low-frequency lock-in techniques). Gate leakage currents were below 10 pA.

Figure 1(a) shows longitudinal MR from a $[\bar{2}33]$ aligned Hall bar at various temperatures. CO are clearly seen at low fields and are accompanied by a positive MR at very low fields. At about 0.3 T the onset of the Shubnikov–de Haas (SdH) oscillations (which modulate the CO) is also seen. As expected, the amplitude of the classically originated CO shows no change in this temperature range, while the SdH oscillations, due to bulk quantization, change considerably. A $\sim$50% fall in the CO amplitude was found on further increasing the temperature from 300 mK to 4 K [electron COs were found to quench at $\sim$40 K (Ref. 5)]. This is expected from the above condition given the hole mass. These data are from a 277-nm deep square QW (*T*212) at -0.5 V gate bias (where the CO appeared most clearly). It is surpris-

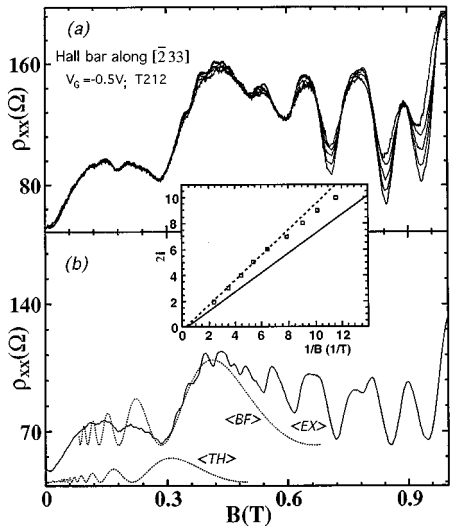

FIG. 1. (a) Magnetoresistance measured between 50 and 300 mK (uppermost trace) in 50 mK increments (traces were shifted along ρ_{xx} to aid comparison). (b) $\langle \mathrm{BF} \rangle$ is a best fit of the theory to the 50 mK trace $\langle \mathrm{EX} \rangle$ (with V_0 matching the first oscillation amplitude). $\langle \mathrm{TH} \rangle$ is the theory curve, with a as the potential period and $k_F=(2\pi p)^{1/2}$ (amplitude is suppressed). Inset: Fan diagram of the position of the CO extrema [seen in (b)] vs B^{-1}. The arbitrary running index i is even (odd) for minima (maxima) in ρ_{xx}. A period of 307 ± 15 nm is obtained on fitting the points, such that both lines coincides at $1/B=0$ using Eq. (1) with $k_F=(2\pi p)^{1/2}$ and the theoretical ϕ values. In comparison, the solid line is obtained using the same ϕ values but the potential period (400 nm).

ing to observe CO from a QW at this depth, for which the grating period-to-depth ratio is only 1.4, as gate definition is expected to decay rapidly with depth. Potential modulation at forward gate biases is primarily due to straining of the GaAs under the slight differential contraction (-0.1%) between metal and substrate as the device is cooled.[6] The CO can be explained by the relatively slow rate of decay with depth of strain (related to the second derivative, with respect to depth, of an electrostatically induced modulation).[6] The CO's are enhanced by the strong coupling between strain and holes at the heterointerface.[7] Nonetheless, the residual strain is insufficient to affect markedly the (311)A band structure.

The positions of the CO extrema, taken from the 50-mK data [Fig. 1(b)], are plotted on a B^{-1} scale versus an arbitrary running index i (see Fig. 1, inset) and show some deviation from linearity, which will be explained later. From the first extrema points we find $\phi=0.19\pm0.06$ for maxima and $\phi=-0.24\pm0.07$ for minima, similar to that found with electrons. The very low field positive MR, found also in electron systems, is seen to extend here to much higher fields. This is expected from the known direct dependence of the field at which the positive MR terminates on m^*.[5] Modeling the experimental field dependence of the CO amplitude correctly requires including $\exp(-\pi/\omega_c\tau)$ as a prefactor to the $\cos^2$ term in Eq. (2).[5] A strong field dependence is therefore expected from the hole's mass, as indeed is seen. However, in contrast to electrons, the experimental CO could not be fitted using the grating period a and $(2\pi p)^{1/2}$, for k_F, in Eq. (2) (p was obtained from the high-field SdH oscillations); the theoretical CO [labeled $\langle \mathrm{TH} \rangle$ in Fig. 1(b)] are clearly shifted towards lower fields as compared to the experiment. The theoretical relation could be fitted ($\langle \mathrm{BF} \rangle$) using either a p value which is nearly half the actual value, or a period value of 297 ± 3 nm, which is much smaller than the modulation period. However, this discrepancy (which is further evident from Fig. 1, inset) is too large to be accounted for by experimental error in determining a or p and is most likely caused by the definition of k_F. Taking $a=297$ nm and $i=6$, an estimated perimeter $\pi(i+\phi)a$ of 5.4 μm is obtained for the largest cyclotron orbit to produce an MR structure, in agreement with the MFP calculated from the sample mobility.

This discrepancy will be related later to anisotropic (311) A valence-band dispersion. Such anisotropy has also been found by transverse magnetic focusing (TMF),[4] revealing an elliptic Fermi surface (FS) with a slightly flatter dispersion along $[011]$ than along the $[\bar{2}33]$ direction. This anisotropy is traced back to a possible, finely corrugated structure (of 32 Å period) (Ref. 3) at the (311)A heterointerface, which at low fields opens minigaps in the hole dispersion curve along the modulation direction ($[011]$). When disorder and temperatures are low, this could result in a degree of mass enhancement along $[011]$. This FS, however, cannot explain the large mobility anisotropy often found,[4,8] which probably results from an anisotropic scattering time in (311)A.

In a semiclassical model (valid in our case, since $a>\lambda_F$, where λ_F is the Fermi wavelength), under the B field, the motion in k space follows constant-energy contours defined by E_F and corresponds to a real-space orbit with the same shape but rotated by $\pi/2$ and scaled by B^{-1}. Figure 2(a) shows examples of three sets of CO from a series of coprocessed devices fabricated on $T97$, with Hall bars aligned at 0°, 45°, and 75° to the $[\bar{2}33]$ direction. The COs show a clear, *second*-harmonic content (indicated by dashed arrows) as has been previously observed from 2DEG's situated at similar depths from the gate.[9] A striking shift in position of the CO set to lower fields is seen when the Hall bar is ''rotated'' by $\vartheta°$ from $[\bar{2}33]$. Interestingly, the 45° CO set was found to coincide approximately with theory.[10] The field positions of the first three MR peaks from each trace were scaled by the index (i) (i.e., the peaks were normalized such that the $[\bar{2}33]$ points coincided) before being plotted in Fig. 3. The dotted line is an elliptical best fit to the points.[4] It demonstrates the shift away from the expected angularly independent CO positions (solid circle line) which are obtained using k_F, calculated from p, in Eq. (1) [note that employing the relation $k_F=(2\pi p)^{1/2}$ assumes isotropic FS]. A central point here is that this elliptic shape has a similar geometry and size to one quarter of the (311)A Fermi line for the given density (after exchanging $[\bar{2}33]$ and $[011]$ axes, of course), because CO occurs at fields where the Fermi wave vector is given by $k_F=(i+1/4)\pi Bea/h$ for $i=1,2,\ldots$.

Since the two contours (in Fig. 3) can be considered as the experimental and calculated FS (at the given p, to a constant factor), they should enclose the same area, as indeed we find to within 3%. Errors in pinpointing peak positions and Hall-bar directions can account for this discrepancy. This shows that cyclotron orbits producing the SdH oscillations [from which p was determined, to evaluate $k_F=(2\pi p)^{1/2}$ in Eq. (1)] are, unlike CO orbits, affected only by a k_F value aver-

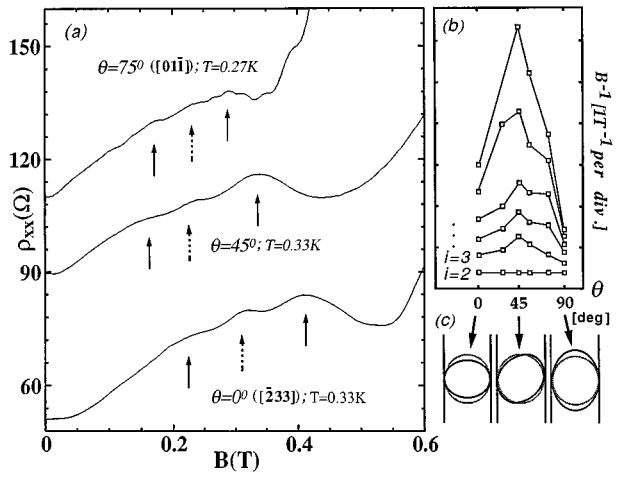

FIG. 2. (a) CO from *T*97 Hall bars along three orientations with 400-nm period grounded gates. Arrows indicate peak positions in field. (b) Extrema positions in B^{-1} vs ϑ (the error is smaller than the point size). Lines connect same index points from all orientations. (c) Elliptic ($i=1$) orbits [derived from the (311)*A* Fermi line shape] commensurate with the grating (vertical lines) are illustrated together with circular orbits (in gray), for $\vartheta=0°$, 45°, 75°. Note that the classically originated CO should not change under slight temperature changes.

aged over all crystallographic directions. It also explains the discrepancy found between the experimental MR traces, and the theory calculated from p. Therefore, for a warped FS, Eqs. (1) and (2) remain valid only if k_F denotes the Fermi wave vector in the direction of the modulation. Since in our near elliptic FS k_F increases with ϑ [reaching a $(2\pi p)^{1/2}$ value at $\vartheta=45°$], the $\cos^2$ argument in Eq. (2) shifts the CO seen in Fig. 2 to lower fields as well as reducing their width. The observed decrease in the CO amplitude with ϑ is due to a strong decrease in the MFP [$\propto \rho_{xx}(0)^{-1}$] with ϑ (note that V_0 is kept constant; all gates are grounded). Mapping out further constant energy contours (of the same set of devices) using this technique of longitudinal magnetic commensurability (LMC) requires changing the Hall bars p. Unfortunately, lowering p by means of applying voltage to the gates would change V_0. This can be avoided by changing E_F (uniformly instead of only below the strip area) via a full back gate or persistent photoconductivity effects, while adjusting V_0 through the front grating gate, such that eV_0/E_F is kept constant (and small).

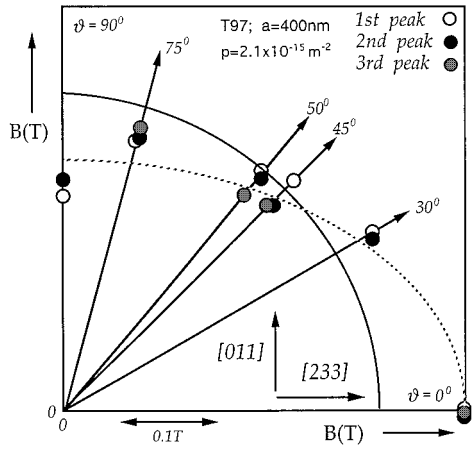

FIG. 3. Angular dependence of the CO sets; corresponding to a near elliptic (311)*A* FS, on exchanging [$\bar{2}$33] and [011] axes (points were slightly displaced in ϑ for clarity). The solid line is the dependence expected from a circular FS.

Plotting the extrema points obtained from all directions on a B^{-1} scale [Fig. 2(b)] reveals deviations from the expected uniformity of point spacing. Connecting points of the same index reveals a peak (at $\sim 45°$) which builds up with i, i.e., as the orbital size increases. Figure 2(c) illustrates that elliptic cyclotron orbits at $\vartheta \sim 45°$ have areas like the circular orbits assumed by theory [Eq. (2)]. Hence, the trend is actually toward a more circular (311)*A* FS as the area probed by LMC grows (with i). This might be because larger orbits are probed from areas containing a greater number of irregularity island defects (in the corrugated structure),[4] which, in turn, further smear the minigap structure and the anisotropic mass enhancement it produces. This can explain the greater FS anisotropy which we find compared to TMF results[4] when extrapolated to our p; even the smallest focusing orbit size they detected ($2R_c \geqslant 1$ μm) would commensurate with our superlattice to produce ρ_{xx} extrema that deviate from a B^{-1} linearity, towards positions expected from circular FS (as is also seen in Fig. 1, inset). In addition, our heterostructures were only doped on one side of the QW (in contrast to Ref. 4); this may further enhance the effect of the corrugations on the holes at the heterointerface. An imperfect well inversion symmetry could also result in a slight lift of Kramers degeneracy. This may explain the unexpected deviation from circular FS for samples with square QW (Ref. 11) that we (in *T*212) and Ref. 4 obtain.

Finally, it is useful to compare the techniques of TMF and LMC; in the former, emitter and collector constrictions have to be defined in the hole gas, which means that the carriers interact with a large potential barrier. In LMC, however, an array of weak barriers ($eV_0 \ll E_F$) only resonantly couple with the motion of the 2D carriers. This makes LMC an appealing, minimally invasive method; additionally, LMC has the potential for higher resolution, as more oscillations can be observed from a given 2DEG. This is because in LMC the number of oscillations which can be observed, for a particular modulation, is determined by the MFP. In TMF, however, the specular reflections of holes from a barrier involves a much shorter hole free path than the conventional elastic MFP evaluated from the sample mobility, and so the number of oscillations that can be observed is rather small. Moreover, unlike TMF, the CO amplitude, and hence LMC resolution, can be increased considerably by changing the grating gate potential slightly (such that the 2D density is almost unchanged). We note that LMC can determine two quarters of the dispersion curve at E_F by just sweeping B in both polarities, whereas the same goal cannot be achieved using the same device in TMF. In this context, a time-averaged observable in a hard-sphere system with bounded motion is always equal to its microcanonical average (from the ergodic theorem).[12] An LMC peak is produced by carrier orbits commensurating with pairs of equidistant strips at many different superlattice regions between the probes. Assuming each of the bounded orbits is intrinsic,[12] it follows that a measurement yielding each LMC trace is equivalent to

measuring a subsystem containing a single electron commensurating over a long period of time. In this sense, LMC data are more statistically significant than the TMF, in which a focusing peak is due to carriers all moving between two focusing constrictions via the same 2D region.

In conclusion, we report 1D COs observed from a 2D hole gas. The higher hole mass and the known mobility anisotropy in (311)*A* distinguish our data from electron data in (100). In particular, we find a near elliptical directional dependence of the oscillations field position. This reflects the FS geometry of the (311)*A* valence band known from TMF studies. This interesting minimally invasive method of utilizing 1D superlattices could, in principle, be used for studying band structures at E_F of non-(100) indexed high-mobility 2D gases.

We thank EPSRC for financial support. B.B. is grateful to K.J. Thomas for technical assistance.

---

*Present address: Toshiba Cambridge Research Centre, 260 Science Park, Milton Road, Cambridge CB3 OHE, United Kingdom.

[1] D. Weiss, K. v. Klitzing, K. Ploog, and G. Weimann, Europhys. Lett. **8**, 179 (1989).

[2] C. W. Beenakker, Phys. Rev. Lett. **62**, 2020 (1989).

[3] R. Notzel, N. N. Ledentsov, L. Dawcritz, and K. Ploog, Phys. Rev. B **45**, 3507 (1992).

[4] J. J. Heremans, M. B. Santos, and M. Shayegan, Surf. Sci. **305**, 348 (1994); J. Appl. Phys. **76(3)**, 1980 (1994); Appl. Phys. Lett. **61**, 1652 (1992).

[5] P. H. Beton, E. S. Alves, and P. C. Main *et al.*, Phys. Rev. B **42**, 9229 (1990); **43**, 9980 (1991); **42**, 9689 (1990).

[6] J. H. Davies and I. A. Larkin, Phys. Rev. B **49**, 4800 (1994).

[7] The modulation produces deformation, similar to that from acoustic phonons, and piezoelectric potentials which scatter at a rate which increases with the carriers mass.

[8] $\mu[\bar{2}33]/\mu[0\bar{1}1]\approx 3$ for the ungated $T97$ (~ 1.4 for $T212$).

[9] R. Cusco *et al.*, Surf. Sci. **305**, 643 (1994).

[10] Given by expanding expressions in Ref. 2 to second order in $\varepsilon = eV_{\rm rms}/E_F$, at the 2DEG as in Ref. 9.

[11] J. P. Eisenstien *et al.*, Phys. Rev. Lett. **53**, 2579 (1984).

[12] D. ter Haar, *Elements of Statistical Mechanics*, 3rd ed. (Butterworth-Heinemann, Oxford, 1995): The theory of Ref. 2 assumes noninteracting Fermi electrons.